ADVANCED OPTICAL MATERIALS
www.advopticalmat.de

Self-Powered Humidity Sensor Using Chitosan-Based Plasmonic Metal–Hydrogel–Metal Filters

Jaehyuck Jang, Kyungnam Kang, Niloufar Raeis-Hosseini, Aizhan Ismukhanova, Heonyeong Jeong, Chunghwan Jung, Byeongsu Kim, Jung-Yong Lee, Inkyu Park, and Junsuk Rho**

A tunable Fabry–Pérot resonator is realized using metal–insulator–metal structure, in which the insulator is chitosan hydrogel. The chitosan swells in response to changes in relative humidity; this change affects transmissive structural color of the multilayer structure. This tunable resonator is utilized for a humidity sensor combined with a photovoltaic cell. The change in current through the photovoltaic cell provides rapid precise measurement of relative humidity, and the change in color of the multilayer provides an approximate, remotely-readable estimate. The response requires no power, so the device has numerous sensing applications.

1. Introduction

Chitosan is a semicrystalline biopolymer derived from chitin,[1] and is biodegradable, biocompatible, and nontoxic.[2] Chitosan-based devices have been evaluated in optics and nanoelectronics,[3,4] particularly as planar optical waveguides for humidity sensors[5] and gas sensors.[6] Chitosan has remarkable film-forming properties,[7] porous structure, and an ability to swell by absorbing water molecules from the air;[8] this change affects both its electrical conductivity and its absorption spectrum. These changes have obvious application as a sensor of relative humidity (RH).

Structural colors found in nature[9] have received great scientific interest and been reproduced by diverse structural colors.[10–12] The simplest structural coloration mechanism consists of planar multilayered arrangements.[13–17] In particular, the metal–insulator–metal (MIM) configuration based on a Fabry–Pérot resonator has a high quality factor efficient band-pass filtering with scalability and cost-effective fabrication.[18–20] However, conventional planar MIM resonators lack tunable function, because the resonance depends only on the geometry and optical parameters of the insulating layer.

Structural colors have been tuned using chemical,[21–26] mechanical,[27,28] or electrical stimuli,[29,30] polarization,[31,32] and phase-change materials.[33] However, tunable structural colors have a slow response,[21] complicated mechanism[27,28,33] and insufficient dynamic change. For those reasons, practical application of structural colors has been limited.

In this work, we propose tunable color filter composed of MIM multilayer, in which the insulator is chitosan hydrogel. This color filter can serve as a humidity sensors when combined with a photovoltaic (PV) cell. The structure uses chitosan film sandwiched between two ultrathin silver (Ag) layers deposited on a glass substrate. The key element is the chitosan insulating layer, in which the effective optical thickness t_{eff} and refractive index n_c change in response to RH; this trait can be exploited to obtain optical tunability of the resonance wavelengths. The corresponding resonance peak shift induces output current change of a PV cell, which is proportional to a change in the RH value of the environment. The special features of the proposed sensor are simple development, incorporation into PV cell, and potentially zero power usage, that make it a promising material for devices that monitor RH in enclosed spaces, workplaces and storage areas.

2. Results and Discussion

2.1. Transfer-Matrix Method (TMM) Simulation of Ag–Chitosan–Ag Multilayer Structures

We present a tunable MIM bandpass filter in which the sensitive insulating layer is composed of chitosan, which can adsorb

J. Jang, Dr. N. Raeis-Hosseini, A. Ismukhanova, C. Jung, Prof. J. Rho
Department of Chemical Engineering
Pohang University of Science and Technology (POSTECH)
Pohang 37673, Republic of Korea
E-mail: jsrho@postech.ac.kr
Dr. K. Kang, Prof. I. Park
Department of Mechanical Engineering
Korea Advanced Institute of Science and Technology (KAIST)
Daejon 34141, Republic of Korea
E-mail: inkyu@kaist.ac.kr
Dr. N. Raeis-Hosseini
Department of Electronics and Electrical Engineering
Imperial College London
London SW7 2AZ, UK
H. Jeong, Prof. J. Rho
Department of Mechanical Engineering
Pohang University of Science and Technology (POSTECH)
Pohang 37673, Republic of Korea
B. Kim, Prof. J.-Y. Lee
School of Energy Environment Water and Sustainability
Korea Advanced Institute of Science and Technology (KAIST)
Daejon 34141, Republic of Korea
The ORCID identification number(s) for the author(s) of this article can be found under https://doi.org/10.1002/adom.201901932.

DOI: 10.1002/adom.201901932

water molecules from the air. The MIM structure mimics a Fabry–Pérot resonator, which has a transparent layer between two reflecting surfaces. In this system, top and bottom 25 nm Ag layers serve as highly reflecting surfaces and chitosan serves as the cavity. Ag is chosen as the material of top and bottom layers because of its low material absorption in the visible regime and potential to excite surface plasmon resonance, and thereby enable high-quality band-pass filtering. The optical response of the resonator, defined as change of the resonant wavelength, is the result of variation of the physical parameters of the cavity, i.e., t_{eff} (nm) and refractive index n_c, in response to change in RH of the local atmosphere (**Figure 1**a). The measured and modeled n_c of chitosan agree well (Figure S1, Supporting Information).

To illustrate the spectra and colors of the filters, we used the TMM to calculate the color gamut and transmission spectra of the samples that had a chitosan layer between Ag layers of 25-nm thickness on a silica substrate. t was varied from 80 to 350 nm in increments of 30 nm. The color gamut of the samples on CIE 1931 Chromaticity Diagram (Figure 1b) showed a broad color spectrum, which can be expected from the high-Q features of a Fabry–Pérot resonator.[17] Calculated transmission spectra were converted to visual representation (Figure 1c, insets at right) by applying a color weighting function (Figure S2, Supporting Information).

The transmission peaks red-shifted as the thickness of the chitosan layer increased (Figure 1c; Figure S3, Supporting Information). To aid in understanding, the electric field distributions (Figure 1d) were obtained for the chitosan layer at the 1st mode of the first sample, the 2nd mode of the seventh sample, and the 3rd mode of the tenth sample.

2.2. Comparison between Calculated and Measured Colors

We performed thickness optimization of chitosan layer to achieve desired the range of t (i.e., 80–210 nm) in the MIM structure (Figure S3, Supporting Information). t was controlled by adjusting the concentration of the chitosan solution and the spin-coating speed. The chitosan solution was spin-coated on the glass substrate with the desired speed, then its thickness was measured using atomic force microscopy (AFM) in contact mode (**Figure 2**a).

We fabricated six MIM filters that used a chitosan layer prepared at spin-coating speeds of 1500–4000 rpm in increments of 500 rpm. Then the thickness of chitosan in each MIM sample was estimated by matching the transmission spectra from UV–vis/IR spectroscopy with those of the simulation (Figure 2b). Overall, the estimated thickness tends to be thicker than that of the chitosan film on the glass substrate (Figure 2a). This discrepancy occurs because the chitosan layer in the sample is thicker in the central part in which the spectra were measured, than in the off-center parts, so the spectra were red-shifted. This argument is supported by the match between the colors extracted from experiments (dashed line) match and the colors in center of optical microscopy images (Figure 2b, insets). Lastly, the experimental values of transmission may be lower than the simulated values because our measurement setup lacked an integrating sphere.

In colorimetric humidity sensor design, the sensing mechanism exploits the swelling/contraction of the polymer, because this response leads to changes of transmission spectra and colors of the multilayer film. In this work, we mainly focus on proof-of-concept of the proposed metal–hydrogel–metal structure as a colorimetric humidity sensor.

2.3. Self-Powered Humidity Sensing with a PV Cell

The changes in t and n_c of the swollen polymer in response to change of the physical parameters of the ambient medium provide a mechanism for sensing applications.[33–35] Here, we combined the MIM filters with a PV cell (**Figure 3**a,b) to achieve scalable RH sensing. The PV cell converts optical response of the filters to an electrical signal. The absorption spectrum of P3HT PV cell has a drastic decrease at wavelengths $600 \leq \lambda \leq 700$ nm (Figure 3c). This decrease enables manipulation of the absorption in the sensing system under varied RH by incorporating an MIM film that has resonance wavelength $\lambda_{res} = 600$ nm. As RH increases, the chitosan layer of sensing film starts to swell, so λ_{res} red-shifts (Figure 3d).

The sensing film used is the 1st sample in Figure 2b. To compensate for the fabrication uncertainties and to take into account decrease in thickness with distance from the center, the initial thickness under ambient condition (RH ≈ 20%) for simulation was set to 155 nm, which is close to the average thickness of the film including the center and off-center parts (Figure 3d). The calculated transmission peaks red-shifted as RH increased, because the chitosan layer swelled. The sensing film affected its absorption of the PV cell, so its output current changed (Figure 3e). Calculations suggest that a change in RH from 7.5% to 83.7% can reduce the light absorption of the PV cell to almost zero. The varied absorption of the PV cells directly affects its output current, and this change can be calibrated to allow estimation of the RH in the immediate environment.

n_c of chitosan also varied with RH (Figure S1, Supporting Information); this change affected both the transmission of the sensing film and the absorption of the PV cell. An increase in RH drove a decrease in n_c, and this change causes a blue-shift of the resonance wavelength, in opposition to the red-shift caused by swelling. This trade-off relation between t_{eff} and n_c affects our device by slowing the shift of λ_{res} as RH increases. However, the blue-shift that is caused by the decrease of n_c is effectively dominated by the red-shift that is caused by swelling of the chitosan, so this trade-off does have a weak influence on the design of the device (Figure S4, Supporting Information).

For a test of the integrated device, we first measured the colors of the sensing film under a range of RH (**Figure 4**a). The color darkened as RH was increased from 7.5% to ≈83.7%; this result is in good agreement with Figure 3d. Next, we estimated the output current of the integrated device with a change of RH from 5% (Dry condition) to 85% with a step of ≈15%. Tests involved a sensing period of 1500 s and a recovery period of 3000 s. As a result of swelling of the chitosan layer, the output current changed under varied humidity conditions (Figure 4b). By the end of each recovery period, the sensing film had contracted back to its initial thickness, as confirmed by return of the output current to the initial level.

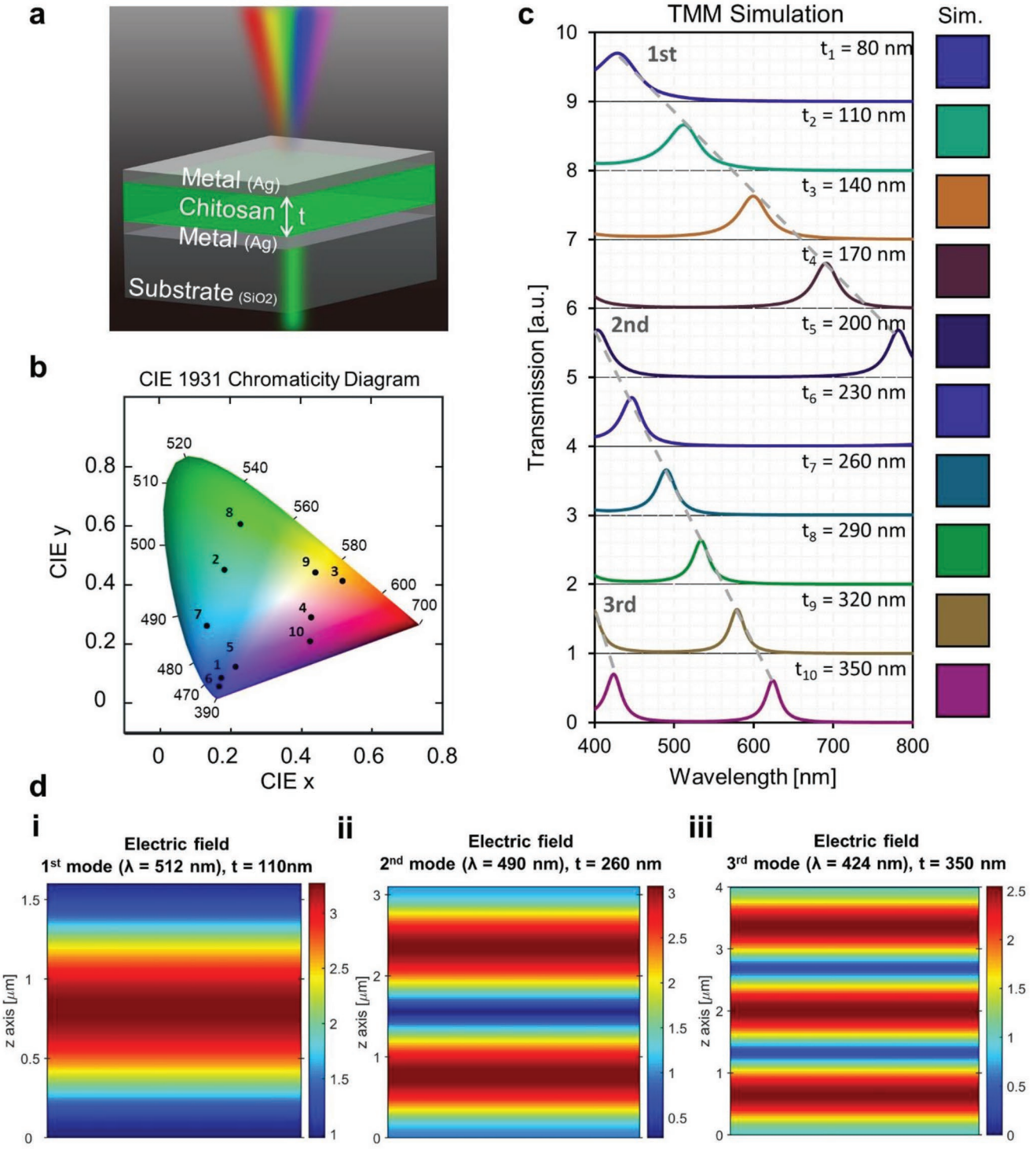

Figure 1. Color gamut, transmission spectra, and field distribution calculated by TMM simulation. a) Schematics of the proposed MIM filter that had thickness *t* of chitosan. b) CIE 1931 chromaticity diagram and c) Transmission spectra of the MIM filters with the varied chitosan thickness (t_n, where *n* is a sample code). Gray dashed lines connect the corresponding modes of Fabry–Pérot resonance (insets: colors of corresponding samples). d) Electric field distribution inside the cavity. (i) 1st mode of the second sample at a wavelength of 512 nm, (ii) 2nd mode of the seventh sample at a wavelength of 490 nm, (iii) 3rd mode of the tenth sample of 424 nm.

To quantify RH, we define the response $\Delta I/I_0$ where ΔI represents the change in electric current from the PV before and after humidity injection, and I_0 is the initial electric initial current in dry (5% RH) N_2 (Figure 4c). The transmission spectra of the sample were recorded before and after the tests (Figure S5, Supporting Information). The first and second tests

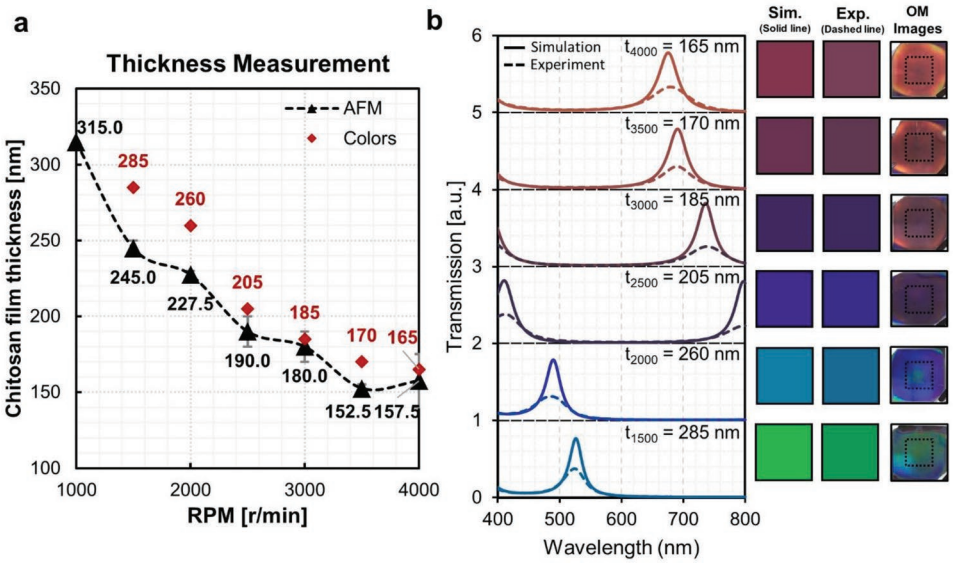

Figure 2. a) Thickness of chitosan with respect to spin-coating speed used to prepare the samples. Thicknesses measured by AFM (triangles) and estimated by structural colors (diamonds). b) Transmission spectra calculated using TMM (solid line) and obtained using UV–vis/IR spectroscopy measurement of MIM filters having estimated thicknesses of chitosan t_ν where ν represents spin-coating speed. Insets: colors converted from simulation and measured spectra, and optical microscopy (OM) images.

yielded slightly different absolute current measurements, possibly due to differences in initial input or environmental condition, but the responses matched well (Figure 4c). Therefore, these responses may correctly indicate the RH in the environment. The trend line can be used to determine the relationship between S and RH h (%) as

$$S = -0.00002h^2 + 0.0046h - 0.0238 \quad (1)$$

with $r^2 = 0.9993$.

To further characterize our sensor, we compared its resolution with those of various types of RH sensors that use chitosan (Table S1, Supporting Information). Our sensor can distinguish a change of 5% RH (Figure S6, Supporting Information). Furthermore, its instant color changes in response to humidity changes enables rough estimation of RH (Figure 4a), so this change in color gives it utility as an instant RH indicator, to complement its accurate RH measurement that can be obtained from the change in output current. Moreover, the sensor does not require a specific light source, and can therefore may be used under arbitrary sources such as sunlight, office fluorescent lamps, and LEDs. The sensor's independence of light source also gives the ability to operate in arbitrary surroundings without any electrical input.

However, our device suffers from a slow response time due to the sandwiched geometry of the chitosan layer. Future work could be aimed to reduce the response and recovery times. One possible design modifications is to change the existing MIM structure to a (metal-nanoparticle)–insulator–metal configuration to facilitate penetration of water vapor through the top layer. This chitosan-integrated device may have optical applications such as a phase modulator tuned by RH (Figure S7, Supporting Information).

3. Conclusion

We proposed a modified tunable Fabry–Pérot system and demonstrated its application in real-time colorimetric humidity sensors. The response of chitosan to the relative humidity of the ambient medium induces dynamic peak shift of the multiple-order resonances in the MIM structures. We calculated transmission spectra of the MIM structure and verified the simulation results by fabricating the device and characterizing it using AFM and UV–vis/IR spectroscopy. Finally, we applied the MIM structure to humidity sensors combined with a PV cell. Output current decreases as RH increases; the response can be described using an equation that can be used to estimate RH. We demonstrate a possible application of the system as a dynamic and real-time colorimetric humidity sensor and expect that the proposed MIM resonator can lead to development of a self-powered sensor.

4. Experimental Section

Materials: Medium-molecular-weight chitosan with a deacetylation degree of 75–85% and molecular weight of 190 000–310 000 Da, acetic acid (AA) (ACS reagent, ≥99.7%) and ammonium hydroxide (NH_4OH) solution (puriss, 30–33% NH_3 in H_2O) were purchased from Sigma-Aldrich and used without further purification. Isopropanol and acetone were purchased from J. T. Baker and used without further purification. A high purity (99.9%) Ag was obtained from E-tek. Glass was diced to a size of 2 cm by 2 cm, and used as substrate for preparing chitosan coatings.

Preparation of Metal Layer: Substrates were cleaned with deionized (DI) water, acetone, and isopropanol, dried using an N_2 gun, then immediately loaded into a plasma cleaner (Cute-b, Femto Science) and placed under vacuum. Ultrathin bottom and top Ag layers were deposited using an E-beam Evaporator System (model KVE-C300160, Korea Vacuum Tech) using a high-purity Ag target under a base pressure of 5×10^{-6} Torr.

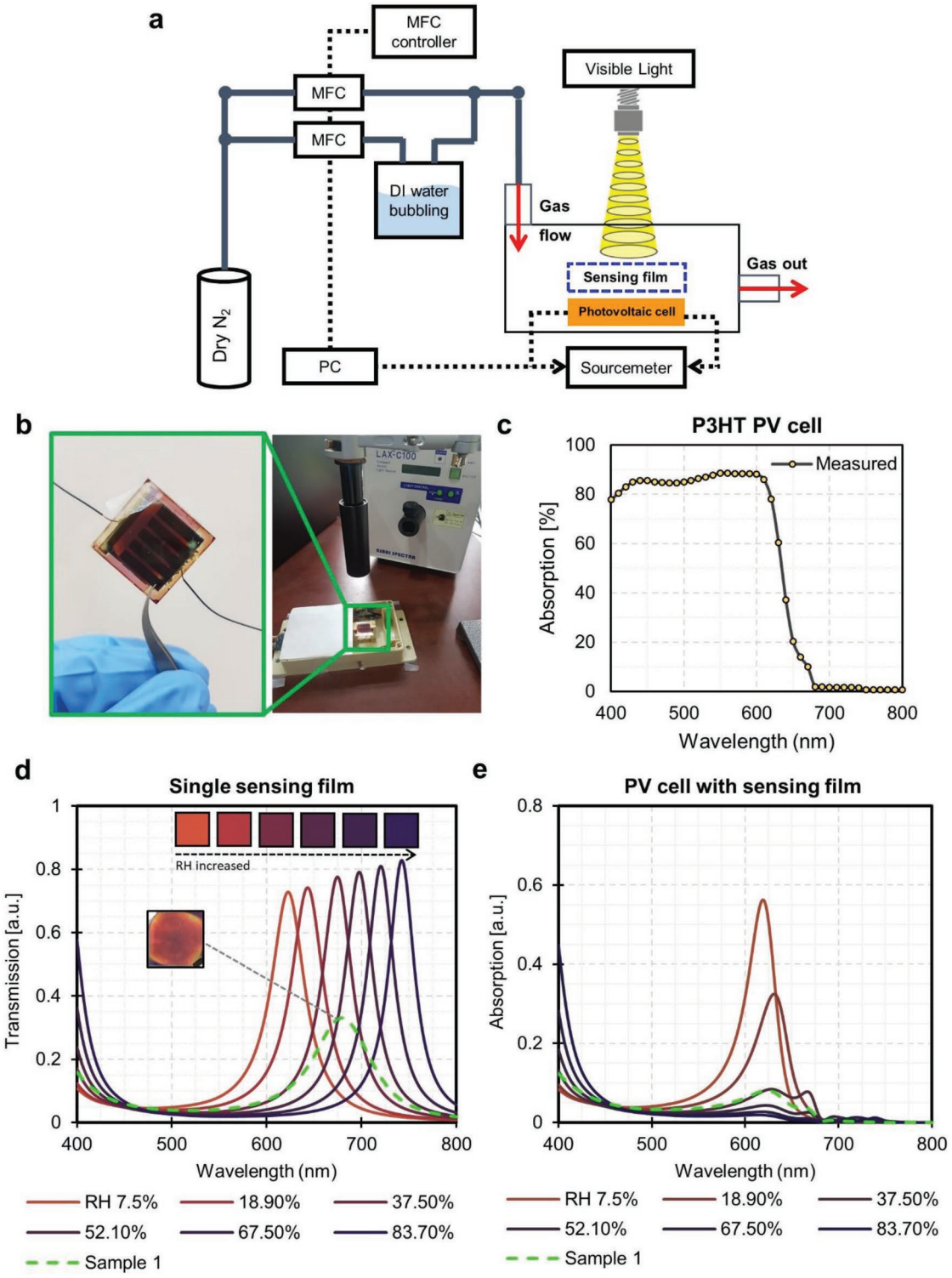

Figure 3. a) Schematic of experimental setup for humidity sensor application. b) Humidity chamber and the sensor device, which is integrated with an organic PV cell and the adaptive MIM filter. c) Measured absorption spectrum of P3HT PV cell used in the sensor. d) Calculated transmission spectra of the single sensing films (solid line) under varied RH conditions and the measured spectra of the sample 1 (dashed line) from Figure 2b. e) Calculated absorption spectra of the PV cell combined with the sensing films as in (b). As the RH is increased, the absorption decreases.

Chitosan Films Fabrication: Chitosan solution with concentration 1.5 wt% was prepared by dissolving the required amount of chitosan powder in 40 mL DI water that contained 1.5 wt% acetic acid. The solution was stirred under heating overnight with 2000 rpm at 65 °C, then centrifuged at 4000 rpm and 25 °C for 3 h. After centrifugation, the solution was preheated at 65 °C for 30 min then filtered through 1.2-µm

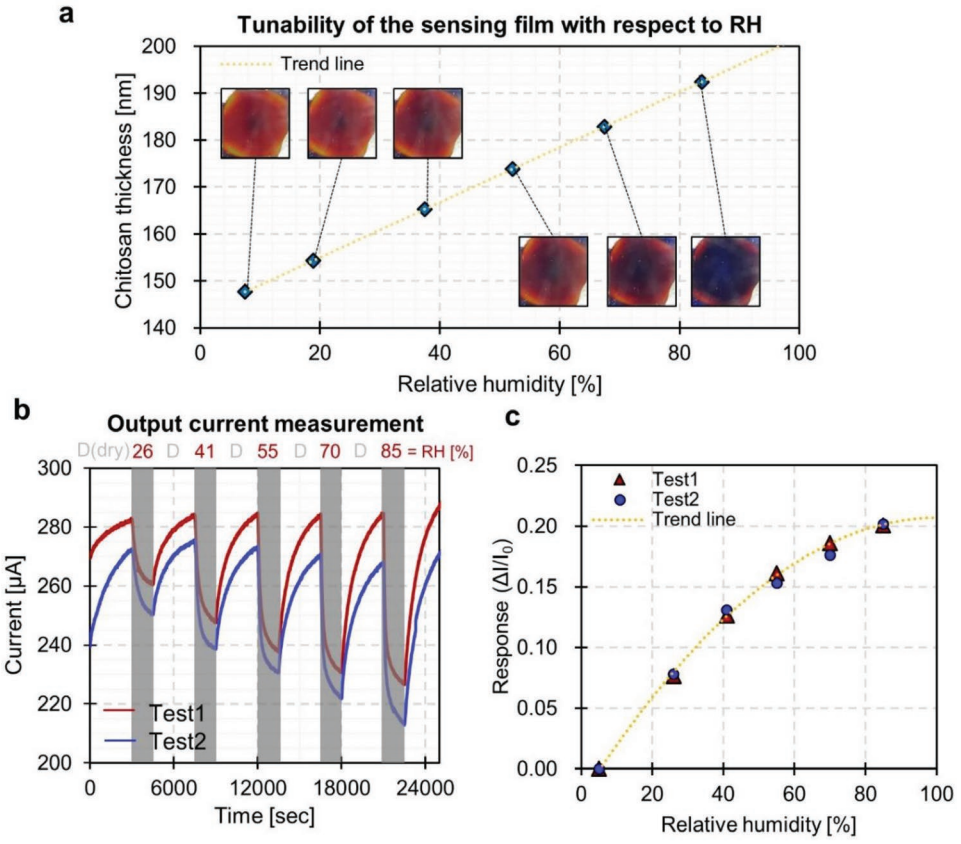

Figure 4. a) Swelling/contraction of the chitosan layer in the sensing film during RH modulation. Insets: corresponding structure colors measured in the chamber. b) Output current generated by the proposed humidity sensor under varied RH condition. Unshaded area: recovery period, shaded area: sensing period. From the current, the film fully regains its original state (RH = 0%) during the recovery period. c) Response of the sensor under varied RH; triangles: Test 1; circles: Test 2; yellow dashed line: trendline of the results.

(25 mm, Sterlitech) and 0.45-μm (13 mm, Whatman) Nylon membrane filters sequentially. To obtain thin polymer films, chitosan solution was spun using a spin-coater onto glass slides (square 20 mm × 20 mm) for 5 s at in 1000 rpm, and then for 2 min at a specified speed. The polymer films were dried at ambient atmosphere for 2 h, then deprotonated by immersion in 3% ammonia solution for 10 min followed by thorough rinsing with distilled water.

Sample Characterizations: Thickness of spin-coated chitosan films on glass wafers was measured in dry state by AFM (Park Systems, XE7). The measurements were performed at ambient humidity (20 ± 5 RH%) and room temperature (20 ± 2°C).

Simulation: Transmission spectra were generated using TMM code developed by the authors. The refractive index of the SiO_2 substrate was set to 1.430. The refractive index of Ag for the simulation was obtained from measured data by Johnson and Christy.[34] Chromaticity simulations were executed using the color-related MATLAB toolbox named OptProp.[35] For color conversions, the CIE 1931 2° observer function with D50 was selected.

Optical Response Measurements: A UV–vis Spectrophotometer (UV-2600Plus, Shimadzu, Japan) was used to measure the transmittance of the chitosan-based MIM filters. The transmittance of samples of various thicknesses (150, 160, 170, 190, 240, and 260 nm) of chitosan was measured with a glass reference. The thickness of chitosan was controlled by the rotation speed of spin-coating. The measurements were conducted at ambient humidity (20 ± 5 RH%) and room temperature (20 ± 2°C).

Stimuli Response Measurements: A xenon light source (LAX-C100, Asahi Spectra, USA) was employed as an ambient light source. The sensor device was placed in a chamber with a transparent window, then various RH (26, 41, 55, 70, 85) of humidity were supplied to the chamber by using a mass-flow controller (MFC). The desired level of humidity was provided by dry nitrogen (N_2) passed into a sealed glass bottle containing deionized water (DI water) and the flow rate was maintained at 500 sccm. To change the RH, dry N_2 gas, and humid N_2 gas passed to DI water were mixed at specific ratio. The RH was confirmed using a humidity sensor (SHT31, Sensirion, Switzerland). The distance between the light source and the sensor device was 100 mm and the intensity of the light source was fixed at 235 W m^{-2}. The output current of organic PV cell was measured using a Sourcemeter (2400, Keithley, USA). The PV cell received no input voltage.

Supporting Information

Supporting Information is available from the Wiley Online Library or from the author.

Acknowledgements

This work was financially supported from Samsung Research Funding & Incubation Center of Samsung Electronics (SRFC-IT1901-05). I.P. acknowledges the National Research Foundation (NRF) grant (NRF-2015R1A5A1037668) funded by the Ministry of Science and ICT (MSIT), Korea. J.J. acknowledges a fellowship from Hyundai

Motor *Chung Mong-Koo* Foundation and the NRF fellowship (NRF-2019R1A6A3A13091132) by Ministry of Education, Korea. A.I. acknowledges the KGSP fellowship funded by the Ministry of Education, Korea.

Conflict of Interest

The authors declare no conflict of interest.

Author Contributions

J.J., K.K., N.R.-H., and A.I. contributed equally to this work. J.R. and N.R.-H. conceived the idea and initiated the project. N.R.-H. did initial design and preliminary experimental work. J.J., A.I., and C.J. continued and developed the simulation and experimental work. B.K. and J.-Y.L. provided the solar cell devices. K.K. and I.P. did the sensor-related work. All authors approved the final version of the manuscript. J.R. guided the entire project.

Keywords

Fabry–Perot etalon, interferometric colors, metal–insulator–metal, structural colors, tunable color filter, tunable structural colors

Received: November 20, 2019
Revised: January 9, 2020
Published online:

[1] M. Rinaudo, *Prog. Polym. Sci.* **2006**, *31*, 603.
[2] M. N. V. Ravi Kumar, *React. Funct. Polym.* **2000**, *46*, 1.
[3] N. Raeis-Hosseini, J.-S. Lee, *Adv. Funct. Mater.* **2015**, *25*, 5586.
[4] N. Raeis-Hosseini, J.-S. Lee, *ACS Nano* **2015**, *9*, 419.
[5] S. S. Voznesenskiy, A. A. Sergeev, A. Yu. Mironenko, S. Yu. Bratskaya, Yu. N. Kulchin, *Sens. Actuators, B* **2013**, *188*, 482.
[6] A. Mironenko, A. Sergeev, A. E. Nazirov, E. Modin, S. S. Voznesenskiy, S. Bratskaya, *Sens. Actuators, B* **2016**, *225*, 348.
[7] T. D. Rathke, S. M. Hudson, J. Macromol. *Sci. Polym. Rev.* **1994**, *34*, 375.
[8] L. H. Chen, T. Li, C. C. Chan, R. Menon, P. Balamurali, M. Shaillender, B. Neu, X. M. Ang, P. Zu, W. C. Wong, K. C. Leong, *Sens. Actuators, B* **2012**, *169*, 167.
[9] P. Vukusic, J. R. Sambles, *Nature* **2003**, *424*, 852.
[10] S. Kinoshita, S. Yoshioka, J. Miyazaki, *Rep. Prog. Phys.* **2008**, *71*, 076401.
[11] I. Kim, G. Yoon, J. Jang, P. Genevet, K. T. Nam, J. Rho, *ACS Photonics* **2018**, *5*, 3876.
[12] T. Lee, J. Jang, H. Jeong, J. Rho, *Nano Converg.* **2018**, *5*, 1.
[13] K.-T. Lee, S. Seo, L. J. Guo, *Adv. Opt. Mater.* **2015**, *3*, 347.
[14] K.-T. Lee, S. Seo, J. Yong Lee, L. Jay Guo, *Appl. Phys. Lett.* **2014**, *104*, 231112.
[15] C.-S. Park, V. R. Shrestha, S.-S. Lee, D.-Y. Choi, *Sci. Rep.* **2016**, *6*, 25496.
[16] Y.-T. Yoon, S.-S. Lee, *Opt. Express* **2010**, *18*, 5344.
[17] H. Kwon, S. Kim, *ACS Photonics* **2015**, *2*, 1675.
[18] M. A. Kats, F. Capasso, *Laser Photonics Rev.* **2016**, *10*, 735.
[19] M. Qin, M. Sun, R. Bai, Y. Mao, X. Qian, D. Sikka, Y. Zhao, H. J. Qi, Z. Suo, X. He, *Adv. Mater.* **2018**, *30*, 1800468.
[20] S. Banisadr, A. Oyefusi, J. Chen, *ACS Appl. Mater. Interfaces* **2019**, *11*, 7415.
[21] X. Duan, S. Kamin, N. Liu, *Nat. Commun.* **2017**, *8*, 14606.
[22] T. Xu, E. C. Walter, A. Agrawal, C. Bohn, J. Velmurugan, W. Zhu, H. J. Lezec, A. A. Talin, *Nat. Commun.* **2016**, *7*, 10479.
[23] S. Sun, W. Yang, C. Zhang, J. Jing, Y. Gao, X. Yu, Q. Song, S. Xiao, *ACS Nano* **2018**, *12*, 2151.
[24] X. Duan, N. Liu, *ACS Nano* **2018**, *12*, 8817.
[25] G. Wang, X. Chen, S. Liu, C. Wong, S. Chu, *ACS Nano* **2016**, *10*, 1788.
[26] Y. Chen, X. Duan, M. Matuschek, Y. Zhou, F. Neubrech, H. Duan, N. Liu, *Nano Lett.* **2017**, *17*, 5555.
[27] M. L. Tseng, J. Yang, M. Semmlinger, C. Zhang, P. Nordlander, N. J. Halas, *Nano Lett.* **2017**, *17*, 6034.
[28] P. Gutruf, C. Zou, W. Withayachumnankul, M. Bhaskaran, S. Sriram, C. Fumeaux, *ACS Nano* **2016**, *10*, 133.
[29] K. Xiong, G. Emilsson, A. Maziz, X. Yang, L. Shao, E. W. H. Jager, A. B. Dahlin, *Adv. Mater.* **2016**, *28*, 9956.
[30] K. Xiong, D. Tordera, G. Emilsson, O. Olsson, U. Linderhed, M. P. Jonsson, A. B. Dahlin, *Nano Lett.* **2017**, *17*, 7033.
[31] M. Kim, I. Kim, J. Jang, D. Lee, K. T. Nam, J. Rho, *Appl. Sci.* **2018**, *8*, 982.
[32] J. Jang, H. Jeong, G. Hu, C.-W. Qiu, K. T. Nam, J. Rho, *Adv. Opt. Mater.* **2019**, *7*, 1970016.
[33] F.-Z. Shu, F.-F. Yu, R.-W. Peng, Y.-Y. Zhu, B. Xiong, R.-H. Fan, Z.-H. Wang, Y. Liu, M. Wang, *Adv. Opt. Mater.* **2018**, *6*, 1700939.
[34] P. B. Johnson, R. W. Christy, *Phys. Rev. B* **1972**, *6*, 4370.
[35] optprop – a color properties toolbox – File Exchange – MATLAB Central, http://kr.mathworks.com/matlabcentral/fileexchange/13788-optprop-a-color-properties-toolbox (accessed: February 2018).

